ADVANCED ENERGY MATERIALS
www.advenergymat.de

Effective SEI Formation via Phosphazene-Based Electrolyte Additives for Stabilizing Silicon-Based Lithium-Ion Batteries

Adjmal Ghaur, Christoph Peschel, Iris Dienwiebel, Lukas Haneke, Leilei Du, Laurin Profanter, Aurora Gomez-Martin, Martin Winter, Sascha Nowak, and Tobias Placke**

Silicon, as potential next-generation anode material for high-energy lithium-ion batteries (LIBs), suffers from substantial volume changes during (dis)charging, resulting in continuous breakage and (re-)formation of the solid electrolyte interphase (SEI), as well as from consumption of electrolyte and active lithium, which negatively impacts long-term performance and prevents silicon-rich anodes from practical application. In this work, fluorinated phosphazene compounds are investigated as electrolyte additives concerning their SEI-forming ability for boosting the performance of silicon oxide (SiO_x)-based LIB cells. In detail, the electrochemical performance of NCM523 || SiO_x/C pouch cells is studied, in combination with analyses regarding gas evolution properties, post-mortem morphological changes of the anode electrode and the SEI, as well as possible electrolyte degradation. Introducing the dual-additive approach in state-of-the-art electrolytes leads to synergistic effects between fluoroethylene carbonate and hexafluorocyclotriphosphazene-derivatives (HFPN), as well as enhanced electrochemical performance. The formation of a more effective SEI and increased electrolyte stabilization improves lifetime and results in an overall lower cell impedance. Furthermore, gas chromatography-mass spectrometry measurements of the aged electrolyte with HFPN-derivatives as an additive compound show suppressed ethylene carbonate and ethyl methyl carbonate decomposition, as well as reduced *trans*-esterification and oligomerization products in the aged electrolyte.

1. Introduction

In the last decades, lithium-ion battery (LIB) technology has dominated the market for portable electronic devices due to its outstanding properties including high energy density, long lifetime, high safety, and low cost per energy content.[1] Additionally, LIBs were introduced in the automobile sector to realize affordable and performant electric vehicles (EVs) that can compete with cars powered by internal combustion engines.[2] To achieve broader customer acceptance, there is a considerable demand for battery technologies with much higher energy densities (Wh L^{-1}) than today.[3,4]

Silicon (Si) is the most promising anode material for LIBs to replace the state-of-the-art graphite anode, as it offers notably higher theoretical volumetric and gravimetric capacities (2190 mAh cm^{-3}; 3579 mAh g^{-1}) compared to graphite (759 mAh cm^{-3}; 372 mAh g^{-1}).[5,6] In addition, Si is the second most abundant element on earth, making it economically attractive for battery applications.[7] On the flip side, Si suffers from a vast volume expansion (≈300%) during the (de)lithiation process, which limits the application of pure Si in LIBs due to particle cracking and pulverization of the active material, loss of electronic contact, and thereby notable capacity fading.[8,9] In addition, continuous breakage and re-formation of the solid electrolyte interphase (SEI) in each cycle leads to a remarkable loss of electrolyte and active lithium.[10,11] To overcome such challenges, tremendous efforts have been attempted lately. Small amounts of Si (up to ≈3–8 wt%; often in the form of SiO_x) embedded in a graphite matrix with effective binders is a promising approach for enhanced electrochemical performance.[12–14]

To further improve cell performance, SEI-forming additives like fluoroethylene carbonate (FEC) and vinylene carbonate (VC) are often employed in the electrolyte.[15–18] Still, Si volume changes during (de)lithiation result in poor Coulombic efficiencies (C_{Eff}) due to ineffective SEI formation, thus limiting practical application. An ideal SEI should be built up during the first cycle(s) via the decomposition of solvents and salts and protect the anode with an, in the ideal case, electronically insulating and ionically conducting layer, as well as prevent contact between the electrolyte and the active material, therefore, hindering further electrolyte degradation.[19] Furthermore, the SEI should also ideally

A. Ghaur, C. Peschel, I. Dienwiebel, L. Haneke, L. Du, L. Profanter, A. Gomez-Martin, M. Winter, S. Nowak, T. Placke
MEET Battery Research Center
Institute of Physical Chemistry
University of Münster
Corrensstr. 46, 48149 Münster, Germany
E-mail: agomezma@uni-muenster.de; tobias.placke@uni-muenster.de
M. Winter
Helmholtz Institute Münster
IEK-12
Forschungszentrum Jülich GmbH
Corrensstr. 46, 48149 Münster, Germany
The ORCID identification number(s) for the author(s) of this article can be found under https://doi.org/10.1002/aenm.202203503.

DOI: 10.1002/aenm.202203503

be robust and flexible enough to follow any changes in the particles without breakage. Although many previous scientific publications focused on the capacity decay of Si-based electrodes, there is still no comprehensive understanding of the effects of SEI morphology, composition, and properties on performance. So far, Si-based electrodes studied in cells against metallic lithium with lithium hexafluorophosphate ($LiPF_6$) as electrolyte salt combined with organic carbonate-based electrolytes are the most investigated cell chemistry.[20–24] The main SEI components in these cell systems are reduction products from the typically used mixture (ethylene carbonate [EC]/dimethyl carbonate [DMC]; EC/diethyl carbonate [DEC]; EC/ethyl methyl carbonate [EMC]) of carbonate solvents, as well as lithium fluoride (LiF) as a decomposition product of $LiPF_6$.[20,22,23,25,26] Increasing the amount of LiF in the SEI (with LiF being an inorganic compound) by using various fluorinated electrolyte compounds typically leads to improved electrochemical performance.[27] Surface investigations by Jaumann et al.[28] on Si/carbon nanocomposite electrodes with FEC, as well as investigations of FEC and VC as electrolyte additives reported by Nguyen et al.[29] showed that a thin polymeric layer (poly(VC); poly(FEC)) among other decomposition products (LiF, lithium carbonate, lithium alkyl carbonates) on the top of the SEI surface can increase the properties of an effective film formation layer further. It has been reported for Li metal battery (LMB) and LIB anodes that inorganic and organic SEI components show different effects in regard to ion transport and electron-insulating SEI properties.[30–32] Investigations on the SEI formation by Michan et al.[23] indicated similar reduction products for FEC and VC. Still, with different relative quantities of Li_2CO_3, $Li_2C_2O_4$, HCO_2Li, and poli(VC), they suggested that the relative amounts of organic and inorganic environments of the SEI likely have an impact on the Li^+ transport mechanism.

Alternative additive compounds, such as dioxolone derivatives, have been proposed for future LIBs, but only a few have been investigated for Si-based electrodes.[33,34] The use of a non-fluorinated additive compound has been reported by Nölle et al.[35] to improve the electrochemical performance in NCM111 ($LiNi_{0.33}Co_{0.33}Mn_{0.33}O_2$) || Si full-cells by using 5-methyl-1,3-dioxolane-2,4-dione (lacOCA), a compound with two functional SEI active moieties. This newly designed additive mixture improved the electrochemical performance in terms of capacity retention and C_{Eff} by forming Li_2CO_3 and poly-(lactid acid) as a thin polymer layer on the SEI surface.

Janssen et al.[36] reported on bi-functional interphase forming additives improving SEI and cathode electrolyte interphase (CEI) properties. Schmiegel et al.[37] reported a study of *N*-carboxy anhydrides (NCAs) as additive compounds with two SEI active moieties, which improved the electrochemical performance and notably reduced the gassing during the SEI formation and posterior cycling. All the relevant reports in the literature emphasize that the nature of the SEI plays an essential role in the long-term stability of LIB cells, and the last two mentioned reports clarify that it is possible to tailor electrolyte additives but also the SEI by changing the molecular structures of SEI active compounds.

Considering the gained insights into the SEI morphology and the property of previously applied compounds to modify the SEI properties, cyclic fluorinated phosphazene compounds, such as ethoxy(pentafluoro)cyclotriphosphazene (EtPFPN) **1**, hexafluorocyclotriphosphazene (HFPN) **2**, and pentafluoro(phenoxy)cyclotriphosphazene (PhPFPN) **3**, might be suitable candidates to form an effective SEI on Si-based anode materials (**Figure 1**). Cyclic phosphazene compounds are commonly known to undergo a ring-opening polymerization to form a linear phosphazene string or an oligo-ring structure and have previously been explored as flame retardants for organic electrolytes in LIBs.[38–41] Recently, Liu et al.[42] successfully demonstrated a cooperative film formation strategy of the anode and the cathode side with ethoxy(pentafluoro) cyclotriphosphazene in $LiNi_{0.5}Mn_{1.5}O_4$ (LNMO) || Li metal cells. They reported the formation of the SEI on Li metal and a P-, N-rich CEI on LNMO.

In this work, the synergistic effect of fluorinated phosphazene compounds in combination with FEC (Figure 1) as electrolyte additives on the electrochemical performance of NCM523 ($LiNi_{0.5}Co_{0.2}Mn_{0.3}O_2$) || SiO_x/C pouch cells is analyzed. Their SEI forming ability at the Si anode side, the storage behavior at elevated temperatures, the gas generation during the formation procedure and after long-term cycling, as well as the electrolyte aging are thoroughly investigated. Additionally, post-mortem investigations of the Si anode surface employing X-ray photoelectron spectroscopy (XPS) and scanning electron microscopy (SEM) were performed.

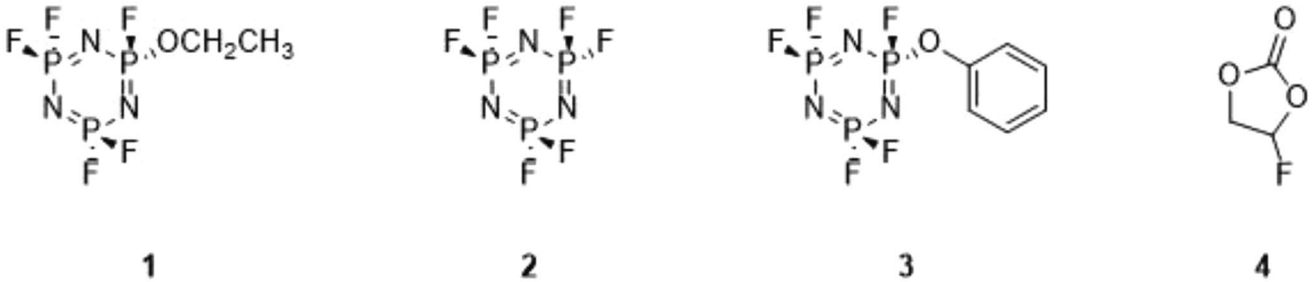

Figure 1. Investigated cyclic phosphazene derivates and FEC as additive compounds in NMC523 || SiO_x/C pouch cells: 1) ethoxy(pentafluoro) cyclotriphosphazene (EtPFPN), 2) hexafluorocyclotriphosphazene (HFPN), 3) pentafluoro(phenoxy)cyclotriphosphazene (PhPFPN), 4) fluoroethylene carbonate (FEC).

2. Results and Discussion

2.1. Electrochemical Behavior of Electrolyte Formulations Containing HFPN-Derivatives

To investigate the effect of HFPN-derivatives in different electrolyte formulations, NCM523 || SiO_x/C multi-layered pouch cells (10 wt% SiO_x content) were charged/discharged 700 times, and electrochemical parameters were systematically analyzed (**Figure 2**). The specific capacities of all cells containing different electrolyte formulations (see **Table 1** for details) were normalized to that of the first discharge cycle. The normalized discharge capacities of the cells are depicted in Figure 2A.

As can be seen, there is a strong capacity fading at the beginning of the experiments for all cells. This capacity fading is expected to be mainly caused by the notable volume expansion of the Si-based negative electrode in the NCM523 || SiO_x/C cells, which accelerates particle cracking, parasitic side reactions, and ongoing consumption of base electrolyte, electrolyte additive, and active lithium from NCM523.[43] The cells using the STD electrolyte (Table 1) undergo a continuous decay and reach 70% state-of-health ($SOH_{70\%}$) after only 170 cycles. The cells with only HFPN-derivatives as electrolyte additives performed better than the STD electrolyte ones. The cells containing the electrolyte formulation STD-EtPFPN reach their $SOH_{70\%}$ after 236 cycles, followed by STD-PhPFPN after 226 cycles and STD-HFPN after 217 cycles. The cells containing STD-FEC as electrolyte formulation extends the $SOH_{70\%}$ to 333 cycles and improves the long-term performance by shifting the $SOH_{70\%}$ by 163 cycles compared to the STD blend without an electrolyte additive. The cells containing the dual additive electrolytes, that is, STD-FEC-PhPFPN ($SOH_{70\%}$ after 355 cycles), STD-FEC-EtPFPN ($SOH_{70\%}$ after 395 cycles), and STD-FEC-HFPN ($SOH_{70\%}$ after 412 cycles), were able to shift the $SOH_{70\%}$ to even higher cycle numbers compared to the STD-FEC electrolyte blend. In the dual additive electrolyte formulations (STD-FEC-HFPN-derivatives), one can assume a similar capacity fading to the single additive electrolyte blend (STD-FEC). However, according to our electrochemical results, there is a different course of fading for dual additive electrolyte blends (STD-FEC-EtPFPN, STD-FEC-HFPN, STD-FEC-PhPFPN). Thus, a positive impact on the single additive electrolyte formulation STD-FEC could be observed with HFPN-derivatives. The combination of HFPN-derivatives with FEC could be the reason for the improved electrochemical performance in these dual additive electrolyte formulations.[43]

To get a better understanding of the positive impact of HFPN-derivatives on the electrochemical performance of dual additive electrolytes, the accumulated Coulombic inefficiency (ACIE) was calculated and plotted in Figure 2B. Additionally, the first cycle C_{Eff} of each electrolyte formulation and cycle life to $SOH_{70\%}$ are noted in Table 1. Compared to the STD electrolyte blend without an additive, all other cells containing additional electrolyte additives show a slightly decreased C_{Eff} in the first cycle due to increased active lithium consumption for SEI and possibly CEI formation.[38,42]

Although the STD electrolyte appears to be the most promising electrolyte based on the highest C_{Eff} in the first cycle, the electrochemical trend for the STD electrolyte with ongoing

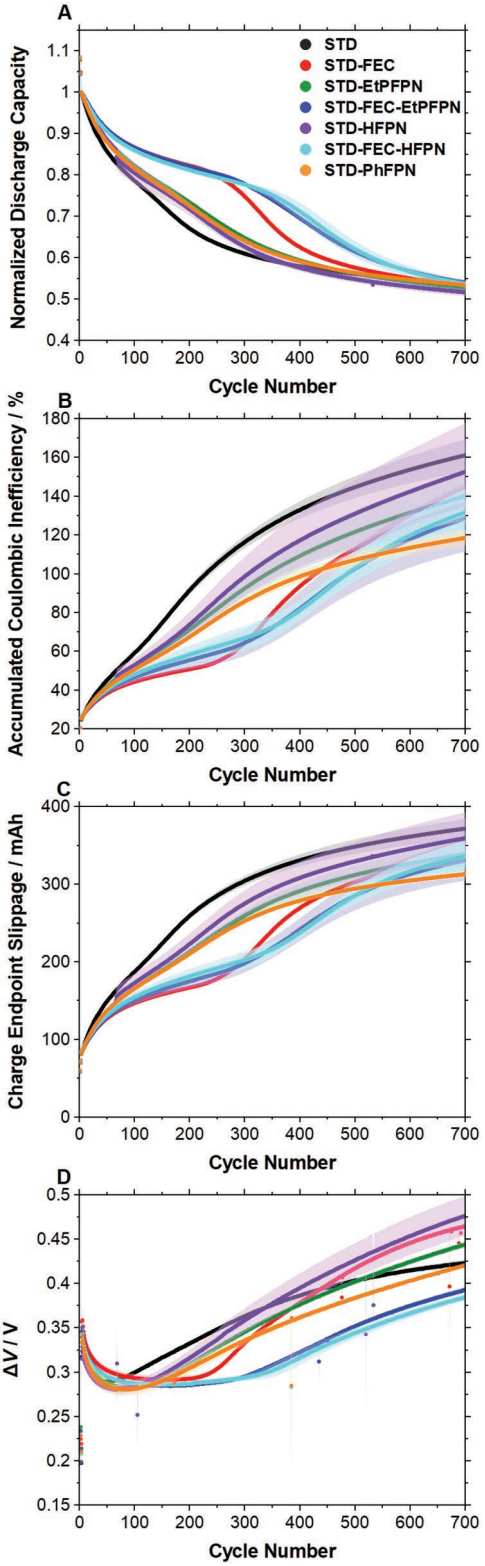

Figure 2. Electrochemical measurements at 20 °C during long-term cycling (2.8–4.3 V at 100 mA (≈0.5 C)) in NCM523 || SiO_x/C pouch cells for different electrolyte formulations: normalized discharge capacity (A), accumulated *Coulombic* inefficiency (ACIE) (B), charge endpoint slippage (C), and cell polarization (Δ*V*) versus cycle number (D). Figures are also shown in the Supporting Information (Figures S1–S4, Supporting Information).

Table 1. Cycle number at $SOH_{70\%}$ and first cycle *Coulombic* efficiency.

Electrolyte Composition	Abbreviation	Cycle number [$SOH_{70\%}$]	C_{Eff} [1st cycle]
1 M $LiPF_6$ in EC:EMC 3:7 by wt%	STD	170	81.2 ± ≤0.1
STD + FEC	STD-FEC	333	80.7 ± ≤0.1
STD + EthoxyPFPN	STD-EtPFPN	236	80.7 ± ≤0.1
STD + FEC + EthoxyPFPN	STD-FEC-EtPFPN	395	80.6 ± 0.1
STD + HFPN	STD-HFPN	217	80.9 ± ≤0.1
STD + FEC + HFPN	STD-FEC-HFPN	412	80.7 ± ≤0.1
STD + PhenoxyPFPN	STD-PhPFPN	226	80.8 ± ≤0.2
STD + FEC + PhenoxyPFPN[a)]	STD-FEC-PhPFPN	355	80.6 ± ≤0.1

[a)]Note, the data concerning STD-FEC-PhPFPN is shown in Figures S5–S9, Supporting Information.

cycling indicates otherwise (Figure 2). Several influential factors, such as Si expansion during the charge and discharge processes, SEI (re-)formation, and enhanced parasitic reactions (shuttle-type reactions, oxidative decomposition, etc.), can reduce the lithium inventory by active lithium consumption, and thus, negatively influence the C_{Eff}.[44] Therefore, to understand the decrease of the C_{Eff} with ongoing cycling, the charge endpoint slippage (Figure 2C) is plotted as an indicator for oxidative and shuttle-type reactions. As can be seen, the STD electrolyte exhibits the highest charge endpoint slippage, followed by STD-HFPN, STD-EtPFPN, and STD-PhPFPN-containing cells. The STD-FEC blend shows the best charge endpoint slippage performance up to ≈260 cycles but then sharply increases. The dual additive electrolyte compositions (STD-FEC-EtPFPN, STD-FEC-HFPN, STD-FEC-PhPFPN) outperformed the STD-FEC blend after ≈260 cycles. However, after ≈600 cycles, the performance of STD-FEC and dual additive electrolytes is similar. The ACIE and the charge endpoint slippage trend indicate that HFPN-derivatives as an additional additive to the STD-FEC blend might be able to stabilize the electrolyte against parasitic reactions.

The difference between the mean charge and the mean discharge voltages (ΔV) is plotted in Figure 2D. It can give an estimation of cell polarization, and thus, cell impedance of different electrolyte compositions upon cycling.[45] All cells show a decreased ΔV value within the first ≈50 cycles after the SEI formation. After 50 cycles, the ΔV value for the STD electrolyte and all single additive-containing electrolytes increase, except for the STD-FEC blend, which has a constant ΔV value until ≈230 cycles. SiO_x cracking and pulverization during the cycling process lead to a thicker SEI formation, and thus, to a polarization of the cell, which is reflected by increased ΔV values. Interestingly, the dual additive approach with STD-FEC-EtPFPN and STD-FEC-HFPN can withstand such polarization up to ≈335 cycles and outperforms the cells containing the STD-FEC electrolyte blend. It is well known that HFPN-derivatives have good film formation/film-forming properties for the anode and the cathode side in specific cell systems like LNMO || Li metal cells.[38,42] Results reported herein support previous investigations, but only in combination with FEC as FEC/HFPN and FEC/EtPFPN. The ΔV plot shows that the additive combination of FEC/HFPN and FEC/EtPFPN has a positive impact on the SEI formation of SiO_x/C electrodes, which is a notable influence factor for the impedance growth in SiO_x/C electrodes upon cycling. HFPN-derivatives alone, without FEC, have shown a moderate impact on the SEI formation on SiO_x/C electrodes. Additionally, a less sharp increase of the ΔV value for both additive combinations (FEC/HFPN, FEC/EtPFPN) indicates a more stable impedance upon cycling. The STD-FEC-PhPFPN blend is not suitable as an electrolyte additive due to increased oxidative and reductive instability upon cycling. In the ΔV versus cycle number plot of the STD-FEC-PhPFPN blend, it can be observed an increased impedance compared to the STD and STD-FEC electrolyte blend, which supports our assumption that the STD-FEC-PhPFPN blend is not able to protect the negative electrode effectively (Figures S5–S8, Supporting Information). Additionally, the open circuit storage experiment at 60 °C for 720 h indicates less oxidative stability for the STD-FEC-PhPFPN formulation (Figure S9, Supporting Information).

2.2. Impact of HFPN-Derivatives on the Gas Evolution Behavior and Electrode Film Formation in NCM523 || SiO_x/C Cells

In previous works, Liu et al.[38,42] reported on the interfacial stability and the film-forming ability of EtPFPN in LNMO || Li metal cells. Here, the gassing behavior of NCM523 || SiO_x/C pouch cells using state-of-the-art electrolytes with cyclic fluorinated phosphazene compounds as additives were investigated regarding their gas-suppressing properties.[46–51] To evaluate the impact of fluorinated cyclic phosphazene-compounds as additives on the gassing behavior, NCM523 || SiO_x/C pouch cells (≈200 mAh cell capacity) were used with a practical electrolyte to cell capacity ratio of ≈4.5 g Ah^{-1}. The gassing behavior for the electrolyte blends with different compositions of phosphazene-derivatives measured by the Archimedes method is illustrated in **Figure 3**A.[46,47] The bulk diagram shows the gas formation of different electrolyte compositions after the SEI formation, after storage at 60 °C for 720 h, and after 700 charge/discharge cycles. Dual additive electrolyte blends show a better gas reduction trend than single additive electrolyte blends, especially for long-term performance. The results for dual additive electrolytes after 700 cycles particularly stand out. The gassing results after 700 cycles were nearly halved for the STD-FEC-EtPFPN blend (0.22 mL) and the STD-FEC-HFPN blend (0.22 mL) compared to the STD-FEC formulation (0.38 mL). The gassing results after storage at 60 °C show a slight decrease for the STD-FEC-EtPFPN blend (gas volume: 0.21 mL) and

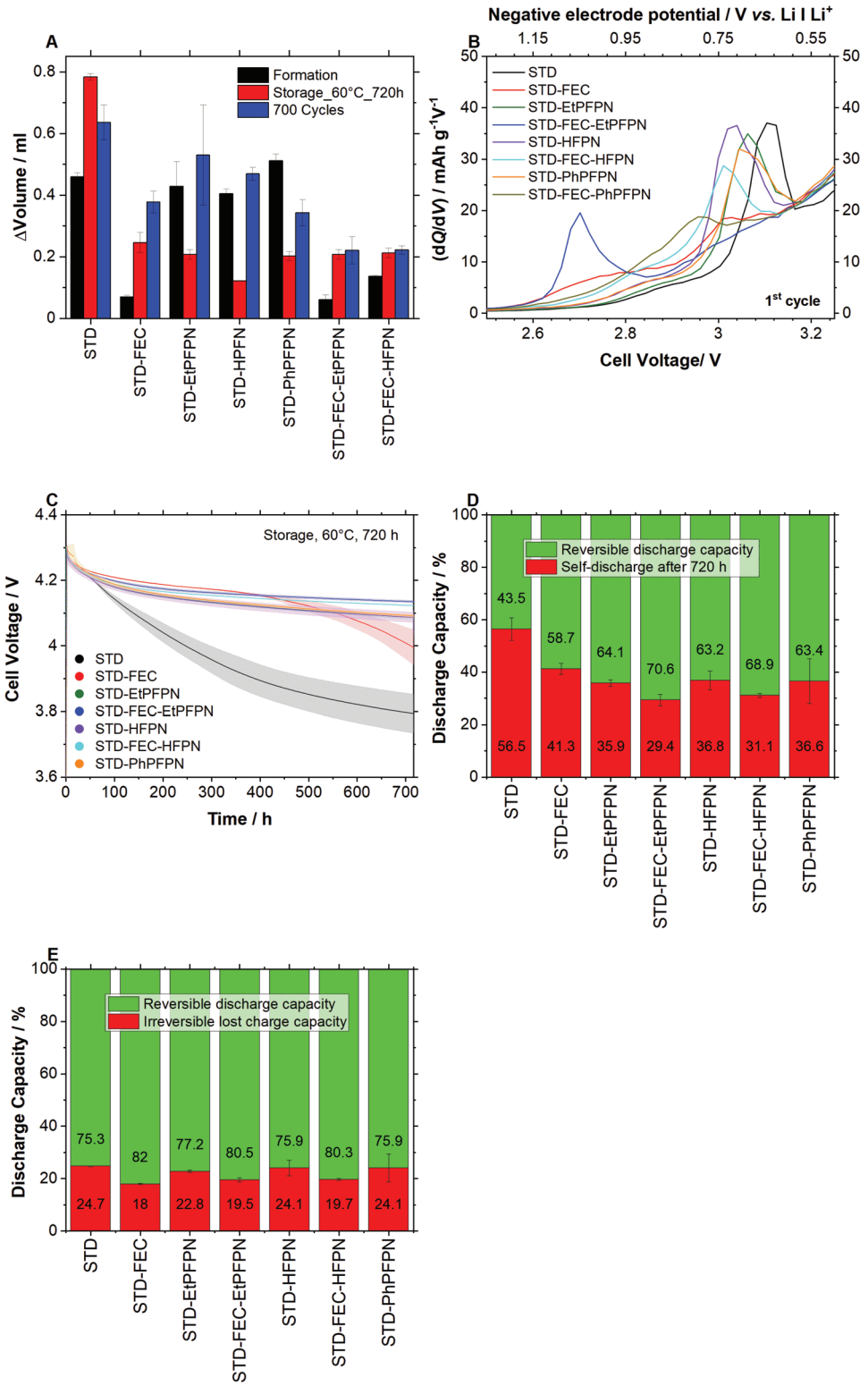

Figure 3. Gas formation in NCM523 || SiO_x/C pouch cells after the formation step, after the storage experiment at 60 °C for 720 h, and after 700 cycles for different electrolyte blends (A). dQ/dV versus cell voltage versus negative electrode potential plots for NCM523 || SiO_x/C pouch cells during formation at 20 °C (B). Voltage drop at 60 °C after 720 h (C). Summary of self-discharge at 60 °C after 720 h (D). Overview of the irreversibly lost charge capacity in a subsequent cycle after 720 h at 60 °C (E). Detailed figures can be found in the Supporting Information (Figures S11–S15, Supporting Information).

STD-FEC-HFPN blend (0.21 mL) compared to the STD-FEC blend (0.25 mL).

As known from the literature, fluorinated phosphazene compounds are typically applied as flame-retardants and tend to have a lower saturated vapor pressure than conventional electrolyte solvents (EC, DEC, DMC, EMC).[38] Our results indicate that fluorinated phosphazene compounds stabilize the electrolyte blend STD-FEC when added as an additional additive, and thus, seem to effectively stabilize conventional electrolyte solvents at high temperatures (60 °C) and during the long-term cycling process. Subsequently, this leads to reduced electrolyte decomposition, less parasitic side reactions, and reduced gas formation (Figure 3A). In contrast to gas formation after the storage experiment and the long-term cycling, the comparison of the dual additive electrolytes STD-FEC-EtPFPN (0.06 mL) and STD-FEC-HFPN (0.14 mL) with the single additive electrolyte STD-FEC (0.07 mL) show similar gassing results after the SEI formation. Based on these gas measurements, it can be assumed that FEC stabilizes the electrolyte in the initial phase during SEI formation. Therefore, the gas measurements after the SEI formation are very similar between STD-FEC and both dual additive electrolyte blends (STD-FEC-HFPN, STD-FEC-EtPFPN). Comparing the gas measurements for STD-FEC after the long-term performance and after the storage experiments with the dual additive blends indicate that FEC as an additive cannot stabilize the electrolyte in the long-term storage process and the long-term cycling process. In contrast, the STD-FEC-HFPN blend and the STD-FEC-EtPFPN blend can stabilize the electrolyte more effectively during the SEI formation and during the long-term cycling, and at high temperatures (Figure 3C); thus FEC/EtPFPN and FEC/HFPN complement each other in the dual additive approach. Gassing during the SEI formation is attributed to electrolyte decomposition. In an EC/EMC-based electrolyte, CO, C_2H_4, and C_2H_6 were mainly detected as generated gases, which can mainly be attributed to EC solvent decomposition.[48] Based on these results in the literature, it is suggested that the decomposition of EC occurred mainly during the initial charging process.[48] According to the gas measurement results shown in Figure 3A, one can assume a reduced EC/EMC decomposition during the SEI formation with the electrolyte formulations containing FEC as an additive compound. To better understand the electrolyte decomposition during the SEI formation, the differential capacity (dQ/dV) versus cell voltage/negative electrode potential for NCM523 || SiO_x/C pouch cells were plotted for the first cycle up to 3.5 V (Figure 3B). A detailed overview of the cell voltage and electrode potential profile of NCM523 || SiO_x/C cells in the first cycle is shown in Figure S10, Supporting Information. An overview of the reductive decomposition of electrolyte additives shown in Figure 3B is provided in **Table 2**.

The STD electrolyte features a reduction onset at a cell voltage of ≈2.72 V (≈1.03 V vs Li|Li$^+$) and a more distinct reduction peak at a cell voltage of ≈3.04 V (≈0.7 V vs Li|Li$^+$). These decomposition peaks can be attributed to EC decomposition to form the SEI at the negative electrode surface.[48–50] In contrast to the STD electrolyte, the STD-FEC blend electrolyte with FEC proceeds through a consecutive broad reduction feature that appears at ≈2.58 V (≈1.17 V vs Li|Li$^+$) and a second reduction peak at ≈2.90 V (≈0.85 V vs Li|Li$^+$), and ends at ≈3.12 V (≈0.63 V vs Li|Li$^+$). The first broad peak can be attributed to FEC decomposition, while the second peak can be attributed to reduced EC decomposition as a major film-forming electrolyte constituent. Compared to the STD electrolyte, the distinct EC decomposition peak at ≈3.04 V (≈0.7 V vs Li|Li$^+$) decreases greatly due to FEC as an additive in the STD-FEC blend, which is known as an effective SEI forming compound with effective protection properties toward further electrolyte reduction.[21,51–55] Additionally, it was possible to observe that there is a shift in the distinct EC decomposition peak from a higher onset cell voltage of ≈3.04 V (≈0.7 V vs Li|Li$^+$ on the potential scale) in the STD electrolyte toward lower onset reductive cell voltage ≈2.90 V (≈0.85 V vs Li|Li$^+$) in the STD-FEC electrolyte blend.[37,61] The introduction of HFPN-derivatives into the STD electrolyte (STD-EtPFPN, STD-HFPN, STD-PhPFPN) features a reduction onset at a cell voltage of ≈2.64 V (≈1.11 V vs Li|Li$^+$), which can be attributed to HFPN-derivatives and a second distinct reduction onset at ≈2.96 V (≈0.79 V vs Li|Li$^+$), which can be attributed to the reductive decomposition of EC. The distinct peaks for the STD-HFPN-derivative blends (STD-EtPFPN, STD-HFPN, STD-PhPFPN) between a voltage of ≈2.96 V (≈0.79 V vs Li|Li$^+$) and ≈3.16 V (≈0.59 V vs Li|Li$^+$), which can be attributed to EC decomposition, show clearly that HFPN-derivatives as a single electrolyte additive alone are not able to reduce EC decomposition notably in the initial SEI formation process (1st cycle). Interestingly, the gas evolving behavior after the SEI formation is similar for the STD electrolyte and the electrolyte compositions with HFPN-derivatives (STD-EtPFPN, STD-HFPN, STD-PhPFPN), which indicates again that HFPN-derivatives are not able to reduce the EC reduction notably, to prevent the generation of gasses (CO, C_2H_4, and C_2H_6) in the initial SEI formation. Thus, the results from the gas measurements in Figure 3A verify the results from the dQ/dV versus cell voltage/negative electrode plot in Figure 3B. On the flip side, the results regarding FEC as a single additive in the STD-FEC blend are in good agreement with our previous assumption that FEC can stabilize the electrolyte in the initial SEI formation process by reducing the EC decomposition; thus, the generation of CO, C_2H_4, and C_2H_6, which are known as main gaseous decomposition products of EC.[48] Further, it was possible to observe that there is a shift in the distinct EC decomposition peak from higher onset cell voltage ≈3.04 V (≈0.7 V vs Li|Li$^+$ on the potential scale) in

Table 2. Reductive decomposition of the investigated electrolyte formulations in Figure 3B.

Electrolyte	Cell Voltage [V]	Anode potential V versus Li|Li$^+$
STD	2.72 and 3.04	1.03 and 0.7
STD-FEC	2.58 and 2.90	1.17 and 0.85
STD-EtPFPN	2.64 and 3.06	0.69 and 0.91
STD-FEC-EtPFPN	2.56	1.19
STD-HFPN	2.64 and 3.04	0.71and 0.91
STD-FEC-HFPN	2.56 and 3.01	1.19 and 0.74
STD-PhPFPN	2.64 and 3.05	0.71and 0.91
STD-FEC-PhPFPN	2.56 and 2.96	1.19 and 0.79

the STD electrolyte toward lower onset reductive cell voltage ≈2.90 V (≈0.85 V vs Li|Li$^+$) with HFPN-derivatives as an additive compound in the STD-HFPN, STD-EtPFPN, and STD-PhPFPN blend.

A similar shift of the reductive decomposition potential to lower cell potential values for EC was observed by introducing FEC and HFPN-derivatives as additives (1:1 molal ratio) in the STD electrolyte to form the dual additive electrolyte blends (STD-FEC-HFPN, STD-FEC-EtPFPN, STD-FEC-PhPFPN). The STD-FEC-HFPN blend shows a broad onset at ≈2.56 V (≈1.19 V vs Li|Li$^+$), which can be attributed to FEC/HFPN decomposition and an EC decomposition peak at ≈3.01 V (≈0.74 vs Li|Li$^+$). The STD-FEC-PhPFPN blend shows a broad onset at ≈2.56 V (≈1.19 V vs Li|Li$^+$), which can be attributed to FEC/PhPFPN decomposition and an EC decomposition peak at ≈2.96 V (≈0.79 V vs Li|Li$^+$). In contrast to these two blends (STD-FEC-HFPN, STD-FEC-PhPFPN), the STD-FEC-EtPFPN blend features only one distinct onset at ≈2.56 V (≈1.19 V vs Li|Li$^+$), which can be attributed to FEC/EtPFPN decomposition. Furthermore, no notable peak could indicate a decomposition of further compounds. One can assume that EC reduction is notably decreased, indicating that the combination of FEC/EtPFPN can form a more effective SEI on the negative electrode surface toward further electrolyte reduction, compared to the STD-FEC electrolyte blend.[38,42] Especially, the gassing behaviors after 700 cycles concerning STD-FEC-EtPFPN and STD-FEC-HFPN show that the continuous decomposition of electrolyte during cycling was reduced, which led to nearly halved volume values in the gas measurements after 700 cycles.[38,42]

For further investigation of the film formation properties, other aspects, such as long-term open-circuit cell voltage (OCV) performance and self-discharge, were also analyzed in NCM523 ‖ SiO_x/C pouch cells. The cell voltages in open circuit conditions are shown in Figure 3C as a function of time for different electrolyte formulations upon storage at 60 °C for 720 h. The storage performance demonstrates the outstanding film formation and electrolyte stabilization properties of the dual additive electrolyte blends (STD-FEC-EtPFPN, STD-FEC-HFPN). Both electrolyte formulations, STD-FEC-EtPFPN (≈4.13 V) and STD-FEC-HFPN (≈4.12 V), were able to protect the electrodes better in comparison to the STD-FEC electrolyte blend (Figure 3C). At 100% state-of-charge (SOC, charging to 4.3 V) and open circuit storage, all cells show a sharp drop of the cell voltage to ≈4.2 V in the initial phase. The self-discharge depends on the SOC; a high SOC results in a higher self-discharge due to accelerated electrolyte oxidation at the positive electrode and shuttle-type reactions (e.g., transition metal dissolution at the positive electrode, transport, and subsequent decomposition at the negative electrode surface) at high voltages.[56,57] Thus, these effects will be noticeable by a sharp drop at the beginning after charging to 4.3 V and will continue during storage.[58] The STD electrolyte shows the most notable cell voltage drop after 720 h (≈3.79 V), while the STD-FEC electrolyte shows a slope of the cell voltage after 400 h. Thus, a cell voltage drop to ≈3.99 V after the long-term open circuit storage can be observed for the STD-FEC blend, whereas all single additive electrolyte formulations with a phosphazene-derivative as an additive performed better and were able to keep the cell voltage moderate during the open circuit storage (STD-EtPFPN ≈4.09 V; STD-HFPN ≈4.09 V; STD-PhPFPN ≈4.04 V). The main reasons for the better storage performance of electrolyte formulations containing only HFPN-derivatives can be i) more effective SEI and CEI formation and ii) the lower saturated vapor pressure of HFPN-derivatives than those of the conventional electrolyte solvents (EC, DEC, DMC, and EMC), which lead to a more stabilized electrolyte at 60 °C. According to our previous observations (cycling data, gas measurement, and dQ/dV vs cell voltage/negative electrode plots), we can suppose that the second reason (ii) is rather responsible for the better storage performance of HFPN-derivatives than the first (i) one. Otherwise, the recorded data in the normalized discharge capacity plot for electrolyte formulations with STD-HFPN-derivatives would be better. Comparing the storage performance via self-discharge (Figure 3D) illustrates the coherence between film formation and capacity retention, but also the coherence between electrolyte stability and capacity retention. While the STD-FEC blend can protect the electrodes properly, the electrolyte stability is lacking at 60 °C due to $LiPF_6$ and FEC instability. Vice versa, STD-HFPN-derivatives can stabilize the electrolyte at 60 °C to prevent $LiPF_6$ instability, but sufficient electrode film formation is lacking. Thus, the lowest self-discharge values were performed with a combination of FEC/EtPFPN as additive compounds in the STD blend, which were able to complement each other again in the STD-FEC-EtPFPN blend. The best storage-performing electrolyte formulation STD-FEC-EtPFPN, with a good film formation property and good electrolyte stability, shows the best capacity retention (≈70.6%) with the lowest self-discharge (≈29.4%) upon 720 h at 60 °C. The capacity retention shows the following order for the other electrolyte blends: STD-FEC-HFPN > STD-EtPFPN > STD-PhPFPN > STD-HFPN > STD-FEC > STD. Based on this trend, it could be observed that good film formation of the positive and negative electrodes, in addition to electrolyte stability by the dual additive approach (FEC/HFPN; FEC/EtPFPN), leads to reduced electrolyte oxidation and shuttle-type reactions. To distinguish between reversible reactions (e.g., electrolyte oxidation, shuttle-type reactions) and irreversible parasitic reactions (e.g., SEI formation), the discharge capacity of fully charged cells at 60 °C in a subsequent cycle after 720 h of OCV storage is shown in Figure 3E. In contrast to the reversible discharge capacity just after storage (Figure 3D), the reversible discharge capacity of the fully charged cells after storage and a subsequent cycle increased (Figure 3E). These results support our assumption that reversible-Li-consuming reactions occur during the storage experiment (e.g., shuttle-type reactions), and thus, directly influence the cell voltage drop (Figure 3C). At the same time, SEI formation does not participate in the voltage drop but contributes to parasitic irreversible Li-consumption, which results in an irreversibly lost charge capacity. However, oxidative decomposition and shuttle-type reactions were reduced in cells containing both additives (FEC/HFPN; FEC/EtPFPN) due to better film formation of the positive and negative electrodes with increased stability of the electrolyte. An increased irreversibly lost charge capacity caused by the SEI formation was observed for cells using HFPN-derivatives as an additive (≈19.5% – ≈24.1%) compared to the STD-FEC electrolyte blend (≈18%) (Figure 3E). The STD electrolyte without an additive causes the highest irreversibly lost charge

capacity (≈24.7%). The second-lowest irreversible lost charge capacity is obtained by the electrolyte formulation STD-FEC-EtPFPN, followed by STD-FEC-HFPN and STD-EtPFPN. The electrolyte formulations STD-HFPN and STD-PhPFPN have equal irreversibly lost charge capacities. In general, SEI- and CEI-forming additives with electrolyte stabilizing properties can protect the electrodes and aim to prevent electrolyte decomposition via oxidation or reduction on the electrode surface.[59,60] When comparing the three dual additive electrolyte blends, the STD-FEC-EtPFPN and the STD-FEC-HFPN blend performed overall better than the STD-FEC-PhPFPN formulation. The gas evolution measurements, storage experiment at 60 °C for 720 h, and cycling data indicate that the additive structure of PhPFPN is mainly responsible for the lower performance.[61] The ortho-phenoxy-group as an electron-donating group destabilizes the core structure of the cyclic phosphazene and tends to be more destabilized in combination with FEC in the STD-FEC-PhPFPN dual additive electrolyte blend. This leads to ineffective film formation on the electrodes, and a destabilized impedance through cycling, due to increased cell polarization, as mentioned previously (Figures S8 and S9, Supporting Information). It was not possible to cycle the cells with the STD-FEC-PhPFPN blend up to ≈700 cycles due to the dry-out of the volatile species. Therefore, gas-evolution measurements for this electrolyte blend were only done after SEI formation and for the storage experiment at 60 °C after 720 h (Figures S16–S18, Supporting Information).

2.3. Ex Situ Surface Investigations of the SiO_x/C Anode Surface

The surface of the negative electrodes was investigated via SEM and XPS to clarify the anode film formation differences between the STD-FEC and STD-FEC-PhPFPN electrolyte blends, which shows the highest difference in the (ΔV) plot (Figure S8, Supporting Information), therefore, enables to better visualize the morphology changes. Furthermore, XPS measurements enable to prove the decomposition of PhPFPN on the negative electrode. Especially, Si-containing anode materials have been reported to intensively consume FEC to form the SEI instead of EC and other electrolytes.[62] Therefore, the surface of SiO_x/C composite electrodes was evaluated in the pristine and different stages of aged cells to elucidate the SEI forming ability and SEI composition with the STD-FEC blend and the STD-FEC-PhPFPN blends.

SEM images of negative electrode surfaces before and after SEI formation and after 200 cycles for the two different electrolyte blends are depicted in **Figure 4**. In the SEM images, SEI formation and SiO_x particle cracking could be clearly detected for both electrolyte blends. Figure 4A1–A3 of the pristine electrode shows a smooth surface of the SiO_x particle (green region, energy dispersion X-ray spectroscopy (EDX)) embedded in graphite (red region, EDX), with some graphite traces on the surface of the SiO_x particle. The electrode surface after the SEI formation with the STD-FEC and the STD-FEC-PhPFPN blend are shown in Figures 4B1–3 and 4C1–3, respectively.

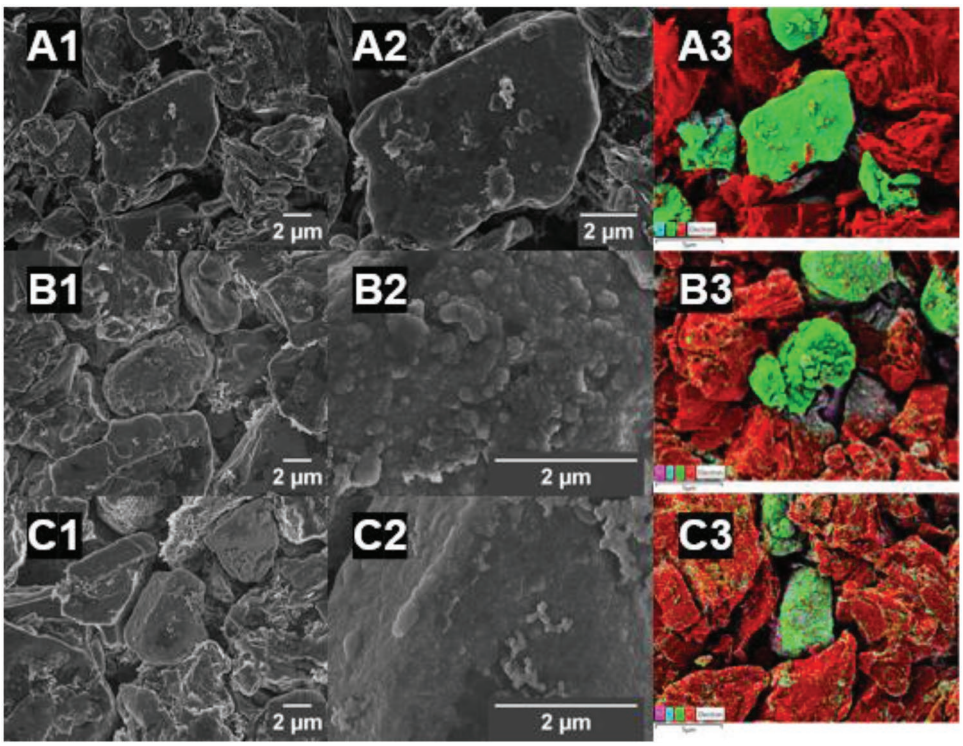

Figure 4. SEM images and EDX measurements of SiO_x/C electrodes of the negative electrode and silicon particles in a pristine state and after SEI formation step with the benchmark STD-FEC blend and the STD-FEC-PhPFPN blend. SEM image of the pristine state (A1,A2) and EDX measurement of the pristine state (A3). SEM images after SEI formation with the benchmark additive STD-FEC (B1,B2) and EDX measurement after SEI formation with the STD-FEC blend (B3). SEM images after the SEI formation with the STD-FEC-PhPFPN blend (C1,C2) and EDX measurements after SEI formation with the STD-FEC-PhPFPN blend (C3).

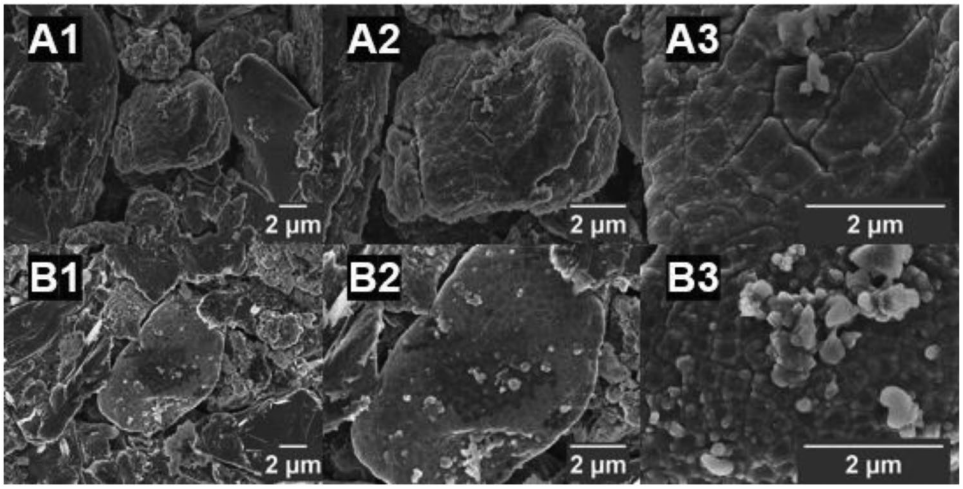

Figure 5. SEM images of SiO_x/C electrodes after 200 cycles with A1–A3) the benchmark additive STD-FEC blend and B1–B3) the STD-FEC-PhPFPN blend.

Interestingly, it is possible to distinguish different morphological features of SEI structure for both electrolyte formulations. The SEI structure with the STD-FEC-PhPFPN blend is relatively smooth compared to the SEI structure with the STD-FEC blend.

Further, the SEI with the STD-FEC-PhPFPN blend is more homogeneous than the SEI with the STD-FEC blend (Figure 4B2,3,C2,3). Additionally, the pulverization of the SiO_x particles (green traces on the red region) is visualized by EDX measurements (Figure 4A3–C3). This observation is in good agreement with previous results in the ΔV plot, where a higher ΔV value was found for the STD-FEC-PhPFPN blend compared to all other electrolyte blends. It can be assumed that the more smooth and more homogeneous morphology of the SEI in the STD-FEC-PhPFPN blend is caused by the increased reductive decomposition of PhPFPN and subsequent decomposition on the anode surface.

SEM images after 200 cycles for both additive blends (STD-FEC, STD-FEC-PhPFPN) are depicted in **Figure 5**. Here, a distinction between the STD-FEC blend (Figure 5A1–3) and the STD-FEC-PhPFPN blend (Figure 5B1–3) could be observed. Cracked SiO_x particle structures were detected in both blends; however, the SEI formation in the STD-FEC blend is less homogenous than that of the STD-FEC-PhPFPN blend. For STD-FEC-PhPFPN-containing cells, these cracked particles appear finer, with fewer deep cracks compared to the STD-FEC blend.[68,41,69] SEM and EDX measurements of the STD-FEC blend after the long-term performance in Figure 2A and measurements of the STD-FEC-PhPFPN blend after the long-term performance in Figure S5, Supporting Information, are provided in the Supporting Information (Figure S19, Supporting Information).

According to the literature, a Li-ion conductive cross-linked poly(FEC) structure on the Si-carbon composite surface is reported for FEC-based additive electrolytes.[29,62] Here, a ring-opening polymerization for the HFPN-derivatives is most likely, leading to a linear poly-phosphazene structure or an oligo ring structure on the SiO_x-carbon composite surface.[41,63]

To investigate the atomic concentration on the SiO_x surface to verify the decomposition of HFPN-derivatives on the negative electrode, XPS measurements of the harvested SiO_x/C electrodes after the SEI formation were measured for PhPFPN and EtPFPN as additional additive compounds to the STD-FEC electrolyte blend, and detailed core spectra for both blends are included in Figures S20 and S21, Supporting Information. The atomic concentration on the top surface layer (≈10 nm) of the negative electrodes was calculated and is shown for both blends in **Figure 6**. XPS measurements of the STD-FEC and the STD-FEC-PhPFPN blends are shown in Figure 6A while those of the STD-FEC and the STD-FEC-EtPFPN blends are compared in Figure 6B. As observed in the XPS core spectra in Figure 6A, nitrogen was not detectable in the STD-FEC electrolyte formulation after the SEI formation and in the soaked sample (STD-FEC-PhPFPN-soaked). At the same time, nitrogen traces (1.6% ± 0.3%) were detected in the STD-FEC-PhPFPN-cycled blend on the negative electrode surface after the SEI formation (Figure S20B, Supporting Information). It can be assumed that these nitrogen residues derive from PhPFPN because PhPFPN is the only nitrogen-containing source in this electrolyte, and the blends were properly opened in an argon-filled glovebox to inhibit nitrogen contamination. Additionally, an increased phosphorus concentration (2% ± 0.4%) was found on the surface of the negative electrodes after the SEI formation with the STD-FEC-PhPFPN-cycled blend (Figure S20A, Supporting Information). $LiPF_6$ is known as a phosphate source, leading to not soluble fluorophosphate and phosphate species on the negative electrode surface.[64] Therefore, phosphate traces could also be found in the STD-FEC electrolyte blend (0.3% ± 0.2%) and the STD-FEC-PhPFPN-soaked sample (0.7% ± 0.1%). Still, according to our data, the phosphorus concentration in the STD-FEC-PhPFPN-cycled blend is much higher than expected and correlates with the nitrogen concentration. It can be supposed that there is PhPFPN decomposition on the anode surface, which could explain the higher concentrations.[65] These observations underpin the possibility of ring-opening polymerization of the PhPFPN core structure to a linear phosphazene polymer

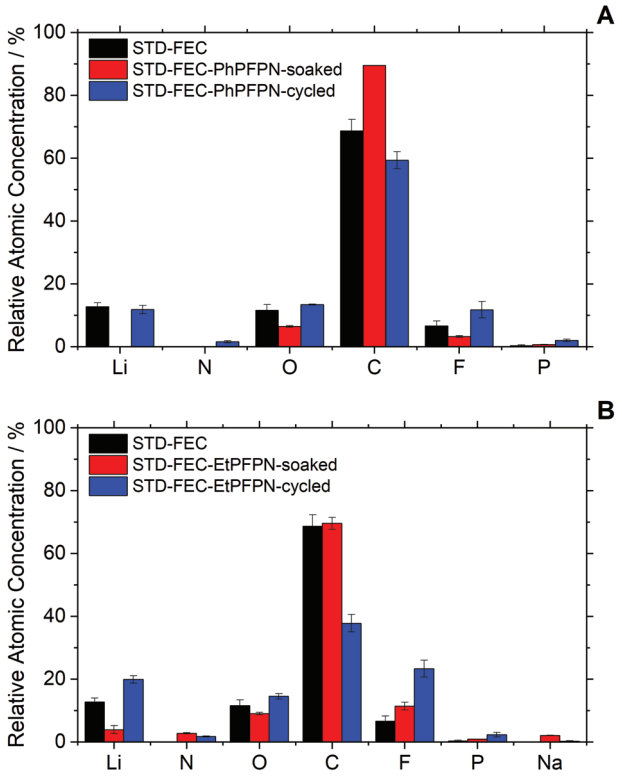

Figure 6. XPS measurements: summary of the atomic concentration on the surface of negative electrodes after the SEI formation in NCM523 || SiO_x/C pouch cells for different electrolyte blends as shown in the legend. A) Relative atomic concentration for PhPFPN as an additional additive compound. B) Relative atomic concentration for EtPFPN as an additional additive compound.

structure or a ring-ring equilibration to an oligo ring structure.[41] Interestingly, in the dual additive approach (STD-FEC-PhPFPN-cycled), the lithium concentration (11.9% ± 1.3%) and the fluorine concentration (11.8% ± 2.6%) on the surface are nearly the same, while the fluorine concentration in the STD-FEC-PhPFPN-cycled blend is higher compared to the STD-FEC blend. The core structure of PhPFPN is fluorinated; therefore, the decomposition of the PhPFPN species on the anode surface would explain the higher measured fluorine concentration. On the other hand, a lower carbon content for the STD-FEC-PhPFPN-cycled blend (59.3% ± 2.7%) implies a lower content of organic SEI species on the negative electrode surface compared to the comparative samples with only FEC as an additive compound (STD-FEC, 68.7% ± 3.6%) and the soaked sample (STD-FEC-PhPFPN-soaked, 89.5%).[68] The oxygen concentration of the STD-FEC blend (11.6% ± 1.8%) is slightly lower compared to the cycled dual additive electrolyte formulation (13.4% ± 0.2%).

In the XPS core spectra in Figure 6B, nitrogen was not detectable in the STD-FEC electrolyte formulation after the SEI formation; however, in the soaked sample (STD-FEC-EtPFPN-soaked), nitrogen was detectable (2.8% ± 0.2%), as well as in the cycled sample, STD-FEC-EtPFPN-cycled (1.8% ± 0.2%). It can be assumed that these nitrogen residues derive from EtPFPN as the only nitrogen-containing source in this electrolyte.

Furthermore, an increased phosphorus concentration was found on the soaked (0.9% ± 0.1%) and the cycled blend (2.3% ± 0.7%) surface of the negative electrodes. Since, $LiPF_6$ is known as a phosphate source, leading to not soluble fluorophosphate and phosphate species on the negative electrode surface, one can assume that $LiPF_6$ is responsible for the slightly higher phosphorus concentration in the cycled blend compared to the soaked blend in Figure 6B.[64]

According to our data, it can be supposed, that there is an EtPFPN deposition on the negative electrode surface, since, nitrogen and increased phosphate traces could be observed in both blends (STD-FEC-EtPFPN-soaked and STD-FEC-EtPFPN-cycled) (Figure S21A,B, Supporting Information). Beyond, in the dual additive approach (STD-FEC-EtPFPN-cycled), the lithium concentration (19.9% ± 1.2%) and the fluorine concentration (23.3% ± 2.7%) on the surface are nearly the same, while the fluorine concentration in the STD-FEC-EtPFPN-cycled blend is nearly three times higher in contrast to the STD-FEC blend (6.6% ± 1.6%) and twice as high as the STD-FEC-EtPFPN-soaked blend (11.4% ± 1.2%). The core structure of EtPFPN is fluorinated; therefore, deposition of the EtPFPN species on the anode surface would explain the higher measured fluorine concentration in the cycled blend. Here, a lower carbon content for the STD-FEC-EtPFPN-cycled blend (37.8% ± 2.8%) also implies a lower content of organic SEI species on the negative electrode surface in contrast to the comparative samples with only FEC as an additive compound (STD-FEC, 68.7% ± 3.6%) and the soaked sample (STD-FEC-EtPFPN-soaked, 69.6% ± 1.9%).[68] The oxygen concentration of the STD-FEC blend (11.6% ± 1.8%) is slightly higher compared to the soaked dual additive electrolyte formulation (9% ± 0.4%), while the oxygen concentration in the cycled dual additive electrolyte blend (14.5% ± 0.9%) is nearly twice as high as the soaked sample (9% ± 0.4%). For EtPFPN as an additional additive compound, sodium could be detected on the negative electrode surface for the soaked blend (2.1% ± 0.1%) and the cycled blend (0.3% ± 0.1%). Since carboxymethyl cellulose (CMC) is used as binder material for the negative electrode in commercial pouch cells, one can assume that CMC is the origin of these sodium peaks.

According to the XPS measurements, it can be postulated that HFPN-derivative decomposition and subsequent deposition on the anode surface take place during SEI formation along with FEC and EC/EMC decomposition products.[46,72] Additionally, in the XPS spectra of the electrolyte blend STD-FEC-EtPFPN-soaked in Figure 6B, it was possible to observe that EtPFPN is able to react with the negative electrode surface in the soaked samples (nitrogen traces), while no nitrogen traces could be observed in the STD-FEC-PhPFPN-soaked samples with PhPFPN as the additional additive compound. This is in good agreement with the electrochemical data and confirms our results. One can assume that the higher surface reactivity of EtPFPN in the STD-FEC-EtPFPN formulation leads to a positive contribution in the SEI formation, thus, improving the electrochemical performance.

2.4. Electrolyte Analysis via Gas Chromatography-Mass Spectrometry

To analyze the decomposition/aging products of the electrolyte at the electrode-electrolyte interface, gas chromatography-mass

spectrometry (GC-MS) measurements were performed. As mentioned above, it is assumed that HFPN-derivatives decomposition along with other electrolyte species (FEC, EC, EMC) takes place on the negative electrode surface to form the SEI. Additionally, HFPN-derivatives were able to stabilize the electrolyte toward higher temperatures. To prove the assumptions indirectly, the decomposition products after the SEI formation and after 700 cycles were analyzed. The STD-PhPFPN additive blend was used as a model compound for HFPN-derivatives and correlated decomposition/aging products. The GC-MS measurements for the STD electrolyte, STD-FEC, and the STD-PhPFPN blend are depicted in **Figure 7**. As indirect proof, one would expect *trans*-esterification and oligomerization products resulting from EC decomposition in the electrolyte during SEI

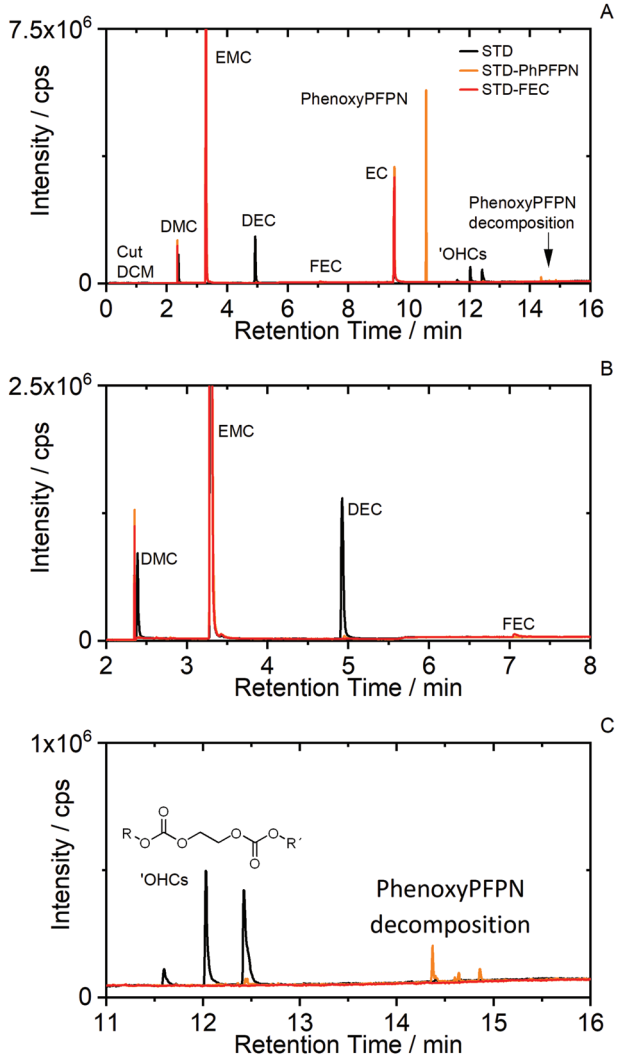

Figure 7. GC-MS of different extracted electrolyte blends after the SEI formation, as shown in the legend. The entire spectrum of the decomposition products (A). Range focused on prominent decomposition peaks (B,C). GC-MS of all other investigated electrolytes is shown in the Supporting Information (Figure S22, Supporting Information). Please note, artificial signals at (2.34) that were originated after the solvent cut for DCM caused by reestablishing the filament voltage do not mix it up with DMC signals, which are slightly shifted afterward.

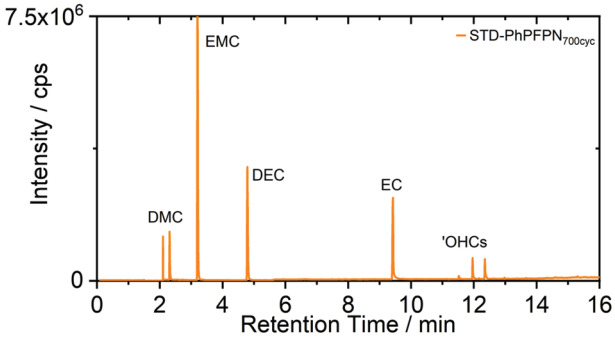

Figure 8. GC-MS of the -PhenoxyPFPN blend after 700 cycles. Please note, artificial signals at (2.10) were originated after the solvent cut for DCM caused by reestablishing the filament voltage, do not mix it up with DMC signals, which is slightly shifted afterward.

formation.[46–51] These *trans*-esterification and oligomerization products ('OHCs) for EC/EMC-based systems are mentioned in the literature as DMC, DEC, ethylmethyl-2,5-dioxahexane-carboxylate (EMDOHC), dimethyl-2,5-dioxahexane-carboxylate (DMDOHC) and diethyl-2,5-dioxahexane-carboxylate (DEDOHC). They have been reported in the literature to cause the generation of gasses and capacity loss in the initial charge process.[48,66–69] Additionally, these species correlated with parasitic reactions deteriorating electrochemical performance and leading to increased impedance growth.[70–72] In Figure 7A, the decomposition of each electrolyte blend can be observed after the SEI formation. Compared to the STD electrolyte blend, the STD-FEC blend and the STD-PhPFPN distinctly decreased the amount of DMC and DEC (Figure 7B), and all mentioned 'OHCs (Figure 7C). These results are in good agreement with observations discussed in the literature concerning film-forming additives at the negative electrode and the formation of *trans*-esterification and oligomerization products upon cycling.[35,37,68,70] Additionally, reduced Li-alkoxide generation at the negative electrode surface could be confirmed, which is associated with the formation of *trans*-esterification products like DEC. Thus, a reduced DEC formation means an indirect reduced Li-alkoxide appearance. With the GC-MS measurements, it was also possible to show the decomposition products of PhPFPN after the SEI formation (Figure 7C).

To better illustrate the long-term aging products of the STD-PhPFPN blend, the electrolyte was also investigated after 700 cycles by GC-MS. PhPFPN was completely consumed after 700 cycles. Consequently, the EC decomposition increased, which led to increased *trans*-esterification products like DEC and oligomerization products like 'OHCs (**Figure 8**). In summary, we can postulate that HFPN-derivatives have a similar effect on aging products like FEC. GC-MS measurements of the STD-EtPFPN blend and the STD-HFPN blend after the SEI formation are deposited in Figure S22, Supporting Information.

3. Conclusion

The cycling performance of NCM523 || SiO_x/C pouch cells in the presence of $LiPF_6$ on organic carbonate electrolytes with and without cyclic fluorinated phosphazene compounds as

film forming and cycling performance stabilizing additives has been investigated. The cooperation of film-forming additives (FEC/HFPN-derivatives) improves the electrochemical performance, stabilizes the electrolyte, and alters the structure of the anode SEI. This approach results in dual additive gas-suppressing electrolytes with the property to notably lower the *trans*-esterification and oligomerization of decomposed cyclic alkyl carbonate and chain alkyl carbonate mixed solvents with $LiPF_6$ as salt in LIBs.[48] The STD blend and the STD-FEC blend do not stabilize the electrolyte toward high temperatures, while the electrolyte blends with the dual additive approach were able to stabilize the electrolyte at high temperatures (60 °C). Furthermore, lower cell impedance could be observed for the STD-FEC-EtPFPN and the STD-FEC-HFPN blend compared to the STD-FEC blend. The relative atomic concentration by XPS measurements of the dual additive electrolyte blends (STD-FEC-PhPFPN and STD-FEC-EtPFPN) on the negative electrode is evidence for HFPN-derivative decomposition. It leads to the assumption that there might be a ring-opening polymerization on the surface, leading to a linear polymeric phosphazene structure or an oligomeric phosphazene ring structure via ring-ring equilibration. Currently, there is no adequate understanding of the expected decomposition mechanism of the fluorinated cyclic phosphazene compounds on the anode surface, nor it is possible to determine the polymeric structure on the surface.

4. Experimental Section

Pouch Cell Setup: Nominally identical, machine-made two-electrode full cells[73] (≈200 mAh capacity, voltage window 2.8–4.3 V) were obtained from Li-Fun Technology. If not otherwise stated, all these cells were composed of $LiNi_{0.5}Co_{0.2}Mn_{0.3}O_2$ (NCM523) positive electrodes and SiO_x/C negative electrodes. Details of the electrodes are provided in **Table 3**. Both sides of the electrodes were coated, except for small regions on one side at the end of the foils. The pouch cells were pre-dried in an oven at 80 °C under reduced pressure (<10^{-3} bar) for 24 h in a dry room (dew point, −80 °C; <0.55 ppm water). After the pre-drying process, the cells were filled with 0.75 mL (≈0.90 g ± 1%) electrolyte and vacuum sealed by heat-crimping at 165 °C for 5 s at a relative pressure of −87 kPa using a vacuum sealer (GN-HS200V, Gelon LIB Group). Custom cell holders with reproducible pressure (2 bar) on the cell stack were used to clamp the cells.[37] A calibrated torque screwdriver was used to fix the custom cell holders and to maintain a pressure of 2 bar.

Electrolyte Compositions: The baseline electrolyte (referred to as STD) containing 1 M $LiPF_6$ in a solution of 3:7 (by weight) EC:EMC (E-Lyte Innovations, 99% pure, less than 20 ppm water). As a benchmark electrolyte additive, 2 wt% FEC (BASF, 98.7% pure), corresponding to 188.59 µmol FEC in 1 g STD electrolyte, was used. The same molal value of FEC (188.59 µmol) was used to calculate the masses of all phosphazene-derivative compounds to ensure the same molal concentration with FEC in all single and dual additive electrolytes. For the single additive electrolyte, three cells for each sample were filled with 0.75 mL ± 1% of electrolyte, containing $LiPF_6$ salt in a solution of 3:7 (by weight) EC:EMC with 188.59 µmol of the additives FEC, ethoxy(pentafluoro)cyclotriphosphazene (EthoxyPFPN, TCI Chemicals, 98% pure), hexafluorocyclotriphosphazene (HFPN, TCI Chemicals, 97% pure), and pentafluoro(phenoxy)cyclotriphosphazene (PhenoxyPFPN, TCI Chemicals, 98% pure). For the dual additive electrolyte, three cells for each sample were filled with 0.75 mL ± 1% of electrolyte-containing $LiPF_6$ salt in a solution of 3:7 (by weight) EC:EMC with a 1:1 (molal ratio) of FEC and each phosphazene-derivate. All chemical compounds were used as derived from the supplier without further purification. The STD electrolyte was prepared in a glovebox (O_2, H_2O <0.1 ppm), transferred in a vacuum-sealed device to the dry room (dew point, −80 °C; <0.55 ppm water) where the additives were added, and the pouch cells were filled with the electrolyte blends. Details of each additive are provided in **Table 4**.

Table 3. Electrode composition of NCM52 || SiO_x/C pouch cells with a polyethylene (PE) one-side coated Al_2O_3 separator.

	Positive Electrode	Negative Electrode
Active material	NCM523 94 wt%	90% AG, 10% SiO_x [85.32 | 9.48 wt%]
Conductive agent	Carbon black, 4 wt%	Carbon black, 1.4 wt%
Binder	PVDF, 2 wt%	CMC, SBR [1.3 | 2.5 wt%]
Mass loading	16.5 mg cm^{-2}	8 mg cm^{-2}
Balanced at cut-off voltage		4.3 V

Electrochemical Cycling Procedure at 20 °C: After filling the pouch cells with electrolyte and after vacuum sealing, they were connected to a battery and cell test equipment with a temperature chamber controlled at 20 °C ± 0.1 °C from MACCOR Inc. For the SEI formation, the Li-Fun cells were held at 1 V for 20 h, charged to 3.5 V at 10 mA (≈0.05 C), followed by a constant voltage (CV) step for 1 h and continued with a discharge to 2.8 V at 10 mA (≈0.05 C). The cells were then charged two times to the upper-cut voltage of 4.3 V at 40 mA (≈0.2 C), at the top of charge (upper-cut voltage), CV was held after each charging process until the current dropped below 4 mA (≈0.02 C) to initiate the discharge process to the lower-cut voltage 2.8 V. After SEI formation, cells were analyzed to quantify the released gas amount using the AISGA methodology. Afterward, the cells were transferred to the dry room, de-gassed, and vacuum-sealed again at the discharged state. For long-term cycling, the pouch cells were charged/discharged between 2.8 and 4.3 V at 100 mA (≈0.5 C) for 700 cycles, if not otherwise stated.[37]

Storage Experiments at 60 °C: The SEI formation procedure and subsequent de-gassing step were the same as the electrochemical cycling procedure mentioned above at 20 °C. For the storage experiments, the pouch cells were connected to the cell test equipment (MACCOR 4000 Series) at 60 °C (temperature-controlled chamber 60 °C ± 0.1 °C) after the SEI formation at 20 °C was completed. The cells were stored for 12 h (OCV), and charged to the upper-cut voltage of 4.3 V. Once the current dropped below 4 mA (≈0.02 C), the OCV was measured for 720 h, then the discharge started to the lower-cut voltage of 2.8 V at 100 mA

Table 4. Composition of the single additive and dual-additive blends in the STD electrolyte.

Electrolyte Additive	FEC	HFPN	EthoxyPFPN	PhenoxyPFPN
Molecular weight/g mol^{-1}	106.05	248.93	275	323.04
Moles/µmol	188.59	188.59	188.59	188.59
Mass per gram electrolyte/mg	20.00	46.95	51.86	60.92
Single additive elec.	FEC	HFPN	EthoxyPFPN	PhenoxyPFPN
Dual additive 1:1 (molal ratio)	–	FEC: HFPN	FEC: EthoxyPFPN	FEC: PhenoxyPFPN

(≈0.5 C). Afterward, the pouch cells were removed from the battery tester, and the gas amount was determined using the AISGA method.[46,37] Afterward, the pouch cells were reconnected to the battery tester at 60 °C and charged/discharged in the first cycle between 2.8 and 4.3 V at 20 mA (≈0.1 C) followed by four cycles between 2.8 and 4.3 V at 100 mA (≈0.5 C), with a CV step at the top of charge until the current dropped below 4 mA (≈0.02 C) to initiate the discharge.

In Situ Gas Volume Measurements: Pouch cells were used in these experiments due to their flexible cell casing, which allowed them to form a bulge if gas was produced during cycling. The details of the measurement methodology to quantify in situ volume change measurements in pouch cells, which is called Archimedes In Situ Gas Analyzer (AISGA), are described elsewhere.[46] For the gas evolution measurements, the pouch cells were submerged in MilliQ water (Merck Millipore Milli-Q Advantage A10, Merck, resistivity 18.2 MΩ cm at 25 °C). At the same time, the cells hung from a balance (S256 Low Range – Force Sensors SMD3277-010, 10 g, Strain Measurement Device) with a wire hook through a ≈1 mm hole in diameter at the sealed edge of the pouch cell. The DAQami v4.2.1 software (Measurement Computing MC, 10 Commerce Way, Norton, MA 0 2766, USA) was used to acquire data and generate signals.

Scanning Electron Microscopy Analysis of SiO_x/C Anodes: The negative electrodes were analyzed via SEM before cycling (pristine), after the SEI formation, and after 700 cycles (aged). Cells were opened after cycling in an argon-filled glovebox (O_2, H_2O contents <0.1 ppm). The SiO_x/C anodes were extracted and rinsed three times with DMC (BASF, battery grade) to remove electrolyte salt residues. To ensure high reproducibility, at least three cells were investigated for each electrolyte formulation. Samples were placed on a vacuum-sealed sample holder and transferred to the SEM chamber without exposure to ambient air. To investigate the SiO_x/C electrode surface morphology of pristine and aged anodes, an SEM (Carl-Zeiss CrossBeam 550, Carl Zeiss Microscopy GmbH) equipped with a field emission gun (Schottky-type) and an in-lens secondary electron detector was used. The working distance for the SEM images was 5.1 mm with an accelerating voltage of 3.5 kV. EDX at an acceleration voltage of 3.5 kV was measured with an Ultim Extrem detector (Oxford Instruments). To evaluate the elemental composition of the samples, AZtech software (Oxford Instruments) was used.

X-ray Photoelectron Spectroscopy Analysis: The pouch cells were opened after the SEI formation procedure in an argon-filled glovebox (O_2, H_2O contents <0.1 ppm), and the electrodes were extracted and rinsed three times with DMC (BASF, battery grade) to remove electrolyte salt residues. The electrodes were placed on the specimen holder and transferred into a special evacuated device to the XPS without exposure to ambient air. To analyze the SEI after formation, an Axis Ultra DLD (Kratos) was used, and fitting was conducted with the CasaXPS software (Version 2.3.16 PR 1.6, Casa Software Ltd.). A monochromatic Al Kα source ($h\nu$ = 1486.6 eV) with a 10 mA filament current and 12 kV accelerating voltage was used. The measurement was conducted at an emission angle of 0° and a pass energy of 40 eV on three positions for each sample. All measurements were performed with an analysis pressure of $<10^{-9}$ mbar. Argon gas was used as the source for the ion gun.

Gas Chromatography-Mass Spectrometry: The aged electrolyte after the SEI formation and >700 cycles at 20 °C was investigated. For that, the pouch cells were opened in a glovebox (O_2, H_2O contents <0.1 ppm) and the electrolytes were extracted via centrifugation of the separator stack. Afterward, electrolyte samples were diluted at 1:100 with DMC prior to measurements to precipitate the conducting salt. GC-MS experiments were performed on a Shimadzu GCMS-QP2010 Ultra device with assembled AOC-5000 Plus autosampler and a nonpolar Supelco SLB-5 ms (30 m × 0.25 mm. 0.25 µm; Sigma Aldrich) column. Further parameters and sample preparation conditions were applied according to Grützke and Mönninghoff et al.[74,75]

Supporting Information

Supporting Information is available from the Wiley Online Library or from the author.

Acknowledgements

The authors wish to thank the Ministry of Economy, Innovation, Digitalization and Energy of North-Rhine Westphalia for funding this work in the project "GrEEn" (313-W044A). The authors would like to acknowledge the work of Empa, Switzerland, their collaboration partner in the Horizon 2020 project SeNSE (grant agreement number 875548), who independently conducted similar experiments and came to similar conclusions.[76]

The acknowledgement to the Horizon 2020 project SeNSE collaboration and the addition of ref [76] were added after initial online publication, on July 14, 2023.

Open access funding enabled and organized by Projekt DEAL.

Conflict of Interest

The authors declare no conflict of interest.

Data Availability Statement

The data that support the findings of this study are available from the corresponding author upon reasonable request.

Keywords

electrolyte additives, lithium-ion batteries, phosphazene compounds, silicon anodes, solid electrolyte interphase

Received: October 17, 2022
Revised: December 18, 2022
Published online: January 4, 2023

[1] P. Bärmann, M. Mohrhardt, J. E. Frerichs, M. Helling, A. Kolesnikov, S. Klabunde, S. Nowak, M. R. Hansen, M. Winter, T. Placke, *Adv. Energy Mater.* **2021**, *11*, 2100925.
[2] J. B. Goodenough, K.-S. Park, *J. Am. Chem. Soc.* **2013**, *135*, 1167.
[3] A. Masias, J. Marcicki, W. A. Paxton, *ACS Energy Lett.* **2021**, *6*, 621.
[4] M. Marinaro, D. Bresser, E. Beyer, P. Faguy, K. Hosoi, H. Li, J. Sakovica, K. Amine, M. Wohlfahrt-Mehrens, S. Passerini, *J. Power Sources* **2020**, *459*, 228073.
[5] R. Teki, M. K. Datta, R. Krishnan, T. C. Parker, T.-M. Lu, P. N. Kumta, N. Koratkar, *Small* **2009**, *5*, 2236.
[6] P. Meister, H. Jia, J. Li, R. Kloepsch, M. Winter, T. Placke, *Chem. Mater.* **2016**, *28*, 7203.
[7] R. Ruffo, S. S. Hong, C. K. Chan, R. A. Huggins, Y. Cui, *J. Phys. Chem. C* **2009**, *113*, 11390.
[8] C. K. Chan, H. Peng, G. Liu, K. McIlwrath, X. F. Zhang, R. A. Huggins, Y. Cui, *Nat. Nanotechnol.* **2008**, *3*, 31.
[9] S. K. Soni, B. W. Sheldon, X. Xiao, M. W. Verbrugge, A. Dongjoon, H. Haftbaradaran, G. Huajian, *J. Electrochem. Soc.* **2011**, *159*, A38.
[10] F. Holtstiege, A. Wilken, M. Winter, T. Placke, *Phys. Chem. Chem. Phys.* **2017**, *19*, 25905.
[11] J. Graetz, C. C. Ahn, R. Yazami, B. Fultz, *Electrochem. Solid-State Lett.* **2003**, *6*, A194.
[12] S. Chae, S. Choi, N. Kim, J. Sung, J. Cho, *Angew. Chem., Int. Ed.* **2020**, *59*, 110.
[13] E. Adhitama, F. D. Brandao, I. Dienwiebel, M. M. Bela, A. Javed, L. Haneke, M. C. Stan, M. Winter, A. Gomez-Martin, T. Placke, *Adv. Funct. Mater.* **2022**, *32*, 2201455.

[14] S. Chae, S. Choi, N. Kim, J. Sung, J. Cho, *Angew. Chem., Int. Ed.* **2020**, *59*, 110.
[15] L. Martin, H. Martinez, M. Ulldemolins, B. Pecquenard, F. le Cras, *Solid State Ion* **2012**, *215*, 36.
[16] V. Etacheri, O. Haik, Y. Goffer, G. A. Roberts, I. C. Stefan, R. Fasching, D. Aurbach, *Langmuir* **2011**, *28*, 965.
[17] Y.-M. Lin, K. C. Klavetter, P. R. Abel, N. C. Davy, J. L. Snider, A. Heller, C. B. Mullins, *Chem. Commun.* **2012**, *48*, 7268.
[18] N.-S. Choi, K. H. Yew, K. Y. Lee, M. Sung, H. Kim, S.-S. Kim, *J. Power Sources* **2006**, *161*, 1254.
[19] E. Peled, *J. Electrochem. Soc.* **1979**, *126*, 2047.
[20] K. W. Schroder, A. G. Dylla, S. J. Harris, L. J. Webb, K. J. Stevenson, *ACS Appl. Mater. Interfaces* **2014**, *6*, 21510.
[21] K. Schroder, J. Alvarado, T. A. Yersak, J. Li, N. Dudney, L. J. Webb, Y. S. Meng, K. J. Stevenson, *Chem. Mater.* **2015**, *27*, 5531.
[22] W. Xu, S. S. S. Vegunta, J. C. Flake, *J. Power Sources* **2011**, *196*, 8583.
[23] B. Philippe, R. Dedryvère, M. Gorgoi, H. Rensmo, D. Gonbeau, K. Edström, *Chem. Mater.* **2013**, *25*, 394.
[24] B. Philippe, R. Dedryvère, M. Gorgoi, H. Rensmo, D. Gonbeau, K. Edström, *J. Am. Chem. Soc.* **2013**, *135*, 9829.
[25] C. K. Chan, R. Ruffo, S. S. Hong, Y. Cui, *J. Power Sources* **2009**, *189*, 1132.
[26] I. Cekic-Laskovic, N. von Aspern, L. Imholt, S. Kaymaksiz, K. Oldiges, B. R. Rad, M. Winter, *Top Curr. Chem.* **2017**, *375*, 37.
[27] V. Etacheri, O. Haik, Y. Goffer, G. A. Roberts, I. C. Stefan, R. Fasching, D. Aurbach, *Langmuir* **2011**, *28*, 965.
[28] T. Jaumann, J. Balach, M. Klose, S. Oswald, U. Langklotz, A. Michaelis, J. Eckert, L. Giebeler, *Phys. Chem. Chem. Phys.* **2015**, *17*, 24956.
[29] C. C. Nguyen, B. L. Lucht, *J. Electrochem. Soc.* **2014**, *161*, A1933.
[30] J. O. Besenhard, M. Winter, *Pure Appl. Chem.* **1998**, *70*, 603.
[31] J. O. Besenhard, M. W. Wagner, M. Winter, A. D. Jannakoudakis, P. D. Jannakoudakis, E. Theodoridou, *J. Power Sources* **1993**, *44*, 413.
[32] M. Winter, *Z. Phys. Chem.* **2009**, *223*, 1395.
[33] S. Park, S. Y. Jeong, T. K. Lee, M. W. Park, H. Y. Lim, J. Sung, J. Cho, S. K. Kwak, S. Y. Hong, N.-S. Choi, *Nat. Commun.* **2021**, *12*, 838.
[34] A. Tornheim, M. He, C.-C. Su, Z. Zhang, *J. Electrochem. Soc.* **2017**, *164*, A6366.
[35] R. Nölle, J.-P. Schmiegel, M. Winter, T. Placke, *Chem. Mater.* **2020**, *32*, 173.
[36] P. Janssen, J. Kasnatscheew, B. Streipert, C. Wendt, P. Murmann, M. Ponomarenko, O. Stubbmann-Kazakova, G.-V. Röschenthaler, M. Winter, I. Cekic-Laskovic, *J. Electrochem. Soc.* **2018**, *165*, A3525.
[37] J.-P. Schmiegel, R. Nölle, J. Henschel, L. Quach, S. Nowak, M. Winter, F. Glorius, T. Placke, *Cell Rep. Phys. Sci.* **2021**, *2*, 100327.
[38] J. Liu, X. Song, L. Zhou, S. Wang, W. Song, W. Liu, H. Long, L. Zhou, H. Wu, C. Feng, Z. Guo, *Nano Energy* **2018**, *46*, 404.
[39] S. V. Sazhin, M. K. Harrup, K. L. Gering, *J. Power Sources* **2011**, *196*, 3433.
[40] C.-K. Kim, D.-S. Shin, K.-E. Kim, K. Shin, J.-J. Woo, S. Kim, S. Y. Hong, N.-S. Choi, *ChemElectroChem* **2016**, *3*, 913.
[41] H. R. Allcock, G. S. McDonnell, J. L. Desorcie, *Inorg. Chem.* **1990**, *29*, 3839.
[42] Q. Liu, Z. Chen, Y. Liu, Y. Hong, W. Wang, J. Wang, B. Zhao, Y. Xu, J. Wang, X. Fan, L. Li, H. bin Wu, *Energy Storage Mater.* **2021**, *37*, 521.
[43] R. Jung, M. Metzger, D. Haering, S. Solchenbach, C. Marino, N. Tsiouvaras, C. Stinner, H. A. Gasteiger, *J. Electrochem. Soc.* **2016**, *163*, A1705.
[44] A. J. Smith, J. C. Burns, D. Xiong, J. R. Dahn, *J. Electrochem. Soc.* **2011**, *158*, A1136.
[45] L. Ma, L. Ellis, S. L. Glazier, X. Ma, Q. Liu, J. Li, J. R. Dahn, *J. Electrochem. Soc.* **2018**, *165*, A891.
[46] C. P. Aiken, J. Xia, D. Y. Wang, D. A. Stevens, S. Trussler, J. R. Dahn, *J. Electrochem. Soc.* **2014**, *161*, A1548.
[47] L. D. Ellis, J. P. Allen, L. M. Thompson, J. E. Harlow, W. J. Stone, I. G. Hill, J. R. Dahn, *J. Electrochem. Soc.* **2017**, *164*, A3518.
[48] H. Yoshida, T. Fukunaga, T. Hazama, M. Terasaki, M. Mizutani, M. Yamachi, *J. Power Sources* **1997**, *68*, 311.
[49] K. Xu, Y. Lam, S. S. Zhang, T. R. Jow, T. B. Curtis, *J. Phys. Chem. C* **2007**, *111*, 7411.
[50] G. V. Zhuang, K. Xu, H. Yang, T. R. Jow, P. N. Ross, *J. Phys. Chem. B* **2005**, *109*, 17567.
[51] E. Markevich, G. Salitra, D. Aurbach, *ACS Energy Lett.* **2017**, *2*, 1337.
[52] V. Etacheri, O. Haik, Y. Goffer, G. A. Roberts, I. C. Stefan, R. Fasching, D. Aurbach, *Langmuir* **2011**, *28*, 965.
[53] K. U. Schwenke, S. Solchenbach, J. Demeaux, B. L. Lucht, H. A. Gasteiger, *J. Electrochem. Soc.* **2019**, *166*, A2035.
[54] F. Aupperle, N. von Aspern, D. Berghus, F. Weber, G. G. Eshetu, M. Winter, E. Figgemeier, *ACS Appl. Energy Mater.* **2019**, *2*, 6513.
[55] V. Etacheri, O. Haik, Y. Goffer, G. A. Roberts, I. C. Stefan, R. Fasching, D. Aurbach, *Langmuir* **2011**, *28*, 965.
[56] S. Klein, L. Haneke, P. Harte, L. Stolz, S. van Wickeren, K. Borzutzki, S. Nowak, M. Winter, T. Placke, J. Kasnatscheew, *ChemElectroChem* **2022**, *9*, 202200469.
[57] A. H. Zimmerman, *IEEE Aerosp. Electron. Syst. Mag.* **2004**, *19*, 19.
[58] N. N. Sinha, A. J. Smith, J. C. Burns, G. Jain, K. W. Eberman, E. Scott, J. P. Gardner, J. R. Dahn, *J. Electrochem. Soc.* **2011**, *158*, A1194.
[59] K. Xu, *Chem. Rev.* **2014**, *114*, 11503.
[60] Y. Qian, S. Hu, X. Zou, Z. Deng, Y. Xu, Z. Cao, Y. Kang, Y. Deng, Q. Shi, K. Xu, Y. Deng, *Energy Storage Mater.* **2019**, *20*, 208.
[61] T. Dagger, M. Grützke, M. Reichert, J. Haetge, S. Nowak, M. Winter, F. M. Schappacher, *J. Power Sources* **2017**, *372*, 276.
[62] R. Jung, M. Metzger, D. Haering, S. Solchenbach, C. Marino, N. Tsiouvaras, C. Stinner, H. A. Gasteiger, *J. Electrochem. Soc.* **2016**, *163*, A1705.
[63] H. R. Allcock, **1988**, 250.
[64] S. Dalavi, P. Guduru, B. L. Lucht, *J. Electrochem. Soc.* **2012**, *159*, A642.
[65] B. S. Parimalam, A. D. MacIntosh, R. Kadam, B. L. Lucht, *J. Phys. Chem. C* **2017**, *121*, 22733.
[66] F. Shi, H. Zhao, G. Liu, P. N. Ross, G. A. Somorjai, K. Komvopoulos, *J. Phys. Chem. C* **2014**, *118*, 14732.
[67] G. Gachot, S. Grugeon, M. Armand, S. Pilard, P. Guenot, J.-M. Tarascon, S. Laruelle, *J. Power Sources* **2008**, *178*, 409.
[68] C. Peschel, F. Horsthemke, M. Winter, S. Nowak, *MethodsX* **2022**, *9*, 101621.
[69] Z. X. Shu, R. S. McMillan, J. J. Murray, *J. Electrochem. Soc.* **1993**, *140*, 922.
[70] J. Henschel, C. Peschel, S. Klein, F. Horsthemke, M. Winter, S. Nowak, *Angew. Chem., Int. Ed.* **2020**, *59*, 6128.
[71] L. M. Thompson, W. Stone, A. Eldesoky, N. K. Smith, C. R. M. McFarlane, J. S. Kim, M. B. Johnson, R. Petibon, J. R. Dahn, *J. Electrochem. Soc.* **2018**, *165*, A2732.
[72] H. Yoshida, T. Fukunaga, T. Hazama, M. Terasaki, M. Mizutani, M. Yamachi, *J. Power Sources* **1997**, *68*, 311.
[73] R. Nölle, K. Beltrop, F. Holtstiege, J. Kasnatscheew, T. Placke, M. Winter, *Mater. Today* **2020**, *32*, 131.
[74] M. Grützke, X. Mönnighoff, F. Horsthemke, V. Kraft, M. Winter, S. Nowak, *RSC Adv.* **2015**, *5*, 43209.
[75] X. Mönnighoff, A. Friesen, B. Konersmann, F. Horsthemke, M. Grützke, M. Winter, S. Nowak, *J. Power Sources* **2017**, *352*, 56.
[76] S. Liu, M. Becker, Y. Huang-Joos, H. Lai, G. Homann, R. Grissa, K. Egorov, F. Fu, C. Battaglia, R.-S. Kühnel, *Batteries & Supercaps* **2023**, *6*, e202300220.